SPE 119104

A Multiscale Mixed Finite-Element Method for Vuggy and Naturally-Fractured Reservoirs

Astrid Fossum Gulbransen, Vera Louise Hauge, and Knut–Andreas Lie, SINTEF ICT

This paper was prepared for presentation at the 2009 SPE Reservoir Simulation Symposium held in The Woodlands, Texas, USA, 2–4 February 2009.

Abstract

Vugs, caves, and fractures can significantly alter the effective permeability of carbonate reservoirs and should be accurately accounted for in a geomodel. Accurate modeling of the interaction between free-flow and porous regions is essential for flow simulations and detailed production engineering calculations. However, flow simulation of such reservoirs is very challenging because of the co-existence of porous and free-flow regions on multiple scales that need to be coupled.

Multiscale methods are conceptually well-suited for this type of modeling as they allow varying resolution and provide a systematic procedure for coarsening and refinement. However, to date there are hardly no multiscale methods developed for problems with both free-flow and porous regions. Our work is a first step to make a uniform multiscale framework in which we develop a multiscale mixed finite-element (MsMFE) method for detailed modeling of vuggy and naturally-fractured reservoirs. The MsMFE method uses a standard Darcy model to approximate pressure and fluxes on a coarse grid, but captures fine-scale effects through basis functions determined from numerical solutions of local Stokes–Brinkman flow problems on the underlying fine-scale geocellular grid. The Stokes–Brinkman equations give a unified approach to simulating free-flow and porous regions using a single system of equations, avoid explicit interface modeling, and reduce to Darcy or Stokes flow by appropriate choices of parameters.

In the paper, the MsMFE solutions are compared with fine-scale Stokes–Brinkman solutions for test cases including both short- and long-range fractures. The results demonstrate how fine-scale flow in fracture networks can be represented within a coarse-scale Darcy flow model by using multiscale elements computed solving the Stokes–Brinkman equations. The results indicate that the MsMFE method is a promising path toward direct simulation of highly detailed geocellular models of vuggy and naturally-fractured reservoirs.

Introduction

Naturally fractured and carbonate reservoirs are composed of porous material, but will typically also contain relatively large void spaces in the form of fractures, small cavities, and caves, which are called *vugs* in the geological literature. Flow simulation of such formations is very challenging because of the co-existence of porous and free-flow domains on multiple scales that require coupling (Wu et al. 2006).

The Darcy–Stokes equations have been used to model industrial infiltration processes and coupled surface and subsurface flow, for which the porous and the free-flow domains are well separated. The Darcy–Stokes model consists of Darcy's law combined with mass conservation in the porous subdomain and the Stokes equations in the free-flow subdomain. To close the model, one must specify conditions on the interface between the Darcy and Stokes subdomains. All such conditions require continuity of mass and momentum over the interface, but differ in the way they allow the tangential component to jump across the interface.

In a carbonate reservoir, the porous and free-flow domains are not well separated: vugs and rock matrix are intertwined throughout the reservoir, often on multiple scales. This means that the coupled Darcy–Stokes approach is not feasible for several reasons. First of all, precise information about the location and geometry of the interface between vugs and the porous matrix is required and also experimentally determined values related to the interface conditions. This information may be possible to obtain for an engineered medium or a small rock sample, but is not possible to obtain for a sector or a full reservoir model. Second, explicit representation of the medium on a centimeter scale, as required to resolve vugs and fractures, would make the flow problem computationally intractable. Finally, the free-flow domains may contain loose fill-in material or particle suspensions in the fluids filling the void space.

When the extent of the hydrocarbon reservoir rock is large, it is therefore not reasonable to apply the Darcy–Stokes equations for the whole domain. Instead, by using tools from homogenization theory, Arbogast and Lehr (2006) predicted that the appropriate macroscopic model would be of Darcy type for which the effective macroscale permeability is derived through upscaling by solving the Darcy–Stokes equations on the microscale within an upscaling block. To treat the block problems, Arbogast and Brunson (2007) designed a mixed finite-element formulation with a single set of basis functions that apply for the entire Darcy–Stokes system. (See also (Karper et al. 2008) for an alternative unified discretization). Arbogast and Gomez (2008) recently extended this approach to three spatial dimensions and developed new and efficient multigrid solvers to solve the resulting highly ill-conditioned saddle-point linear system.

Another upscaling approach was recently presented by Popov et al. (2007, 2008) in which the Stokes–Brinkman equations, rather than the Darcy–Stokes equations, are used on the fine scale to compute upscaled effective permeabilities. The Stokes–Brinkman equations can be reduced to either the Stokes or the Darcy equations by appropriate choice of parameters and give a somewhat coarser model that does not require a precise description of the interface between free-flow and porous domains. This is advantageous for applications to real media for which the location of the vug boundaries is uncertain. Moreover, the Stokes–Brinkman model opens up for a seamless transition between Darcy and Stokes, which may be appropriate in damaged zones, etc. Also, from a numerical point-of-view it is attractive to use a single model in which the two domains are represented implicitly through the parameters instead of a two-domain approach involving explicit modeling of the interface between the vuggy and porous domains.

Common for both the upscaling approaches discussed above is that they use a computation on a fine scale to predict effective properties on a coarser scale. Multiscale simulation (Hou and Wu 1997; Juanes and Tchelepi 2008) is an alternative approach that is conceptually well-suited for this type of modeling, as it enables varying resolution and provides a systematic procedure for coarsening and refinement. For Darcy flow, multiscale methods have proved to be more robust than standard upscaling methods (Kippe et al. 2008) and have the advantage that they offer subscale resolution and thus can be used as highly efficient approximate solvers for direct solution of the full fine-scale problem. Multiscale methods have proved capable of handling industry-standard complexity both with respect to grid representation (Aarnes et al. 2008) and flow physics (Lee et al. 2008; Zhou and Tchelepi 2008; Hajibeygi et al. 2008; Krogstad et al. 2009). Natvig et al. (2009) recently demonstrated how multiscale methods can be used to simulate geological models with fracture corridors modeled as volumetric objects with high permeability. To date, however, multiscale methods have not been applied to simulate flow in naturally-fractured and vuggy media using a multiphysics approach with different flow models on the fine and the coarse scale.

This paper presents a multiscale mixed finite-element (MsMFE) method (Chen and Hou 2003; Aarnes 2004) for detailed multiphysics simulation of single-phase flow in naturally-fractured and vuggy reservoirs. The MsMFE method uses a standard Darcy model to approximate pressure and velocity on a coarse grid. Fine-scale effects are captured through basis functions that are determined by solving local Stokes–Brinkman flow problems numerically on the underlying fine-scale geocellular grid. The local flow problems are set up in a way that forces a unit flow across the interface between two coarse blocks, meaning that the corresponding basis functions reduce to the lowest-order Raviart–Thomas (RT0) basis functions for the special case of Darcy flow in a homogeneous medium. In the general case, the basis functions account for local variations of flow velocity resulting from subgrid heterogeneities in the porous domains, increased flow velocities resulting from free-flow domains on the subgrid scale, and geometrical effects in the case of non-square blocks.

The outline of the paper is as follows: We start by introducing the Darcy–Stokes and Stokes–Brinkman models in more details and discuss how to discretize the latter. We then introduce the MsMFE method and assess its utility through a few illustrative numerical experiments, before we round up the paper with some concluding remarks.

Mathematical Models

Incompressible flow in a porous rock matrix typically obeys Darcy's law and is described by a first-order elliptic system in which Darcy's law is combined with a mass-conservation equation to relate the pressure p_D and the total (interstitial) velocity $\vec{u}_D$,

$$\mu \mathbf{K}^{-1}\vec{u}_D + \nabla p_D = \vec{f}, \qquad \nabla \cdot \vec{u}_D = q. \tag{1}$$

Here, μ is the fluid viscosity, $\mathbf{K}$ is the permeability of the porous medium, $\vec{f}$ denotes body forces, and q denotes fluid sources. Eq. 1 may alternatively be manipulated to give a second-order elliptic equation. Incompressible flow in open domains, on the other hand, obeys the Stokes equations,

$$-\mu\nabla \cdot \left(\nabla\vec{u}_S + \nabla\vec{u}_S^{\mathsf{T}}\right) + \nabla p_S = \vec{f}, \qquad \nabla \cdot \vec{u}_S = q. \tag{2}$$

The Stokes–Brinkman equations combine Eqs. 1 and 2 into a single equation,

$$\mu \mathbf{K}^{-1}\vec{u} + \nabla p - \tilde{\mu}\Delta\vec{u} = \vec{f}, \qquad \nabla \cdot \vec{u} = q, \tag{3}$$

where p is the pressure, $\vec{u}$ is the velocity field, $\mathbf{K}$ is a permeability tensor that is equal to the Darcy permeability in the porous subdomain, μ is the viscosity of the fluid, and $\tilde{\mu}$ is an effective viscosity. This model gives a unified approach to model flow in both the free-flow and the porous subdomains using a single system of equations.

In the free-flow (or fluid) domain, we may let $\mathbf{K}$ tend to infinity and set the effective viscosity equal to the fluid viscosity, $\tilde{\mu} = \mu$ to observe that Eq. 3 simplifies to the Stokes equations, Eq. 2. If $\tilde{\mu}$ is set to zero in the porous domains, Eq. 3 simplifies to the coupled Darcy–Stokes equations, which reintroduces the requirement for interface conditions, etc. Instead, we will therefore set $\tilde{\mu}$ equal to the physical fluid viscosity μ. Assume for the moment that the body forces are zero. Then we may rewrite Eq. 3 as

$$\nabla p = -\mu \mathbf{K}^{-1}\vec{u} + \tilde{\mu}\Delta\vec{u}. \tag{4}$$

A comparison of the magnitude of the two velocity terms on the right-hand side shows that the first term dominates the second by several orders of magnitude for typical reservoirs. In other words, Eq. 4 can be seen as Darcy's equation with a small viscosity perturbation. Other choices of $\tilde{\mu}$ are also possible and may provide more accurate modeling; see Popov et al. (2008) for a more thorough discussion.

In the following we will study Eqs. 1 and 3 as our flow models on the coarse and fine scale, respectively. For both models, we will assume no-flow boundary conditions, neglect body forces, and model wells as point sources.

The Multiscale Mixed Finite Element Method

In this section we start by describing the mixed formulation underlying both the MsMFE method and the discretization of the Stokes–Brinkman equations on the fine scale. Then we introduce the MsMFE formulation and describe in some detail the structure of the associated coarse-scale linear systems.

Fine-Scale Discretization and (Hybrid) Linear System. To solve the Darcy equations Eq. 1 on the coarse (and fine for comparison) scale and the Stokes–Brinkman equations Eq. 3 on the fine scale, we will use a mixed finite-element formulation. To this end, we start by assuming that the permeability $\mathbf{K}$ is given as a piecewise constant tensor defined over a regular Cartesian grid in 2D; that is, $\mathbf{K}$ is a constant 2×2 matrix in each cell E_k. Then, for both equations we seek a pair of functions $(\vec{u}, p)$ from a suitable discrete approximation space defined over $\Omega = \bigcup_{k=1}^{N} E_k$ such that $(\vec{u}, p)$ satisfy the variational formulation

$$\begin{aligned} b(\vec{u},\, \vec{v}) - c(p,\, \vec{v}) &= 0, \\ c(\pi,\, \vec{u}) &= (q,\, \pi) \end{aligned} \tag{5}$$

for all test functions $(\vec{v}, \pi)$ from the same discrete approximation space. Here, the bilinear forms are defined as (subscript D for Darcy and SB for Stokes–Brinkman),

$$b_D(\vec{u},\, \vec{v}) = \int_\Omega \mu\vec{v} \cdot \mathbf{K}^{-1}\vec{u}\; d\Omega, \qquad b_{SB}(\vec{u},\, \vec{v}) = \int_\Omega \mu\vec{v} \cdot \mathbf{K}^{-1}\vec{u}\; d\Omega + \int_\Omega \tilde{\mu}\nabla\vec{v} \cdot \nabla\vec{u}\, d\Omega,$$
$$c(p,\, \vec{v}) = \int_\Omega p\, \nabla \cdot \vec{v}\, d\Omega, \qquad (q,\, \pi) = \int_\Omega q\pi\, d\Omega.$$

For the Darcy problem Eq. 1, we use the lowest-order Raviart–Thomas (RT0) elements on the fine grid, for which pressure is in $\mathbb{P}_0$ (i.e., piecewise constant) and the velocity has one degree-of-freedom associated with the normal component on the interface between each pair of grid cells. (That is, $\nabla \cdot \vec{v}$ is constant in $E_i \cup E_j$ and $\vec{v} \cdot \vec{n}$ is constant on $\partial E_i \cap \partial E_j$ and zero on $\partial(E_i \cup E_j)$). On the coarse grid, we will use a set of generalized RT0 basis functions that will be defined in the next subsection. To simplify the coming presentation, we first present the formulation of the hybrid linear system for Darcy flow on the fine scale. To this end, let $\boldsymbol{u}_E$ denote the vector of outward fluxes on the faces of a cell E. Similarly, p_E denotes the pressure at the cell center and $\boldsymbol{\lambda}_E$ the pressures at the cell faces. The mixed finite-element method can then be recast as a local relation between these three quantities,

$$\boldsymbol{u}_E = \boldsymbol{T}_E(p_E - \boldsymbol{\lambda}_E), \tag{6}$$

where $\boldsymbol{T}_E$ is the so-called *transmissibility matrix*. For the mixed method, $\boldsymbol{T}_E$ is a full matrix, whereas for the standard two-point flux-approximation (TPFA) scheme, $\boldsymbol{T}_E$ is diagonal. The local equations, Eq. 6, can now be assembled to form a hybrid system of the form

$$\begin{bmatrix} \boldsymbol{B} & \boldsymbol{C} & \boldsymbol{D} \\ \boldsymbol{C}^{\mathsf{T}} & \mathbf{0} & \mathbf{0} \\ \boldsymbol{D}^{\mathsf{T}} & \mathbf{0} & \mathbf{0} \end{bmatrix} \begin{bmatrix} \boldsymbol{u} \\ -\boldsymbol{p} \\ \boldsymbol{\lambda} \end{bmatrix} = \begin{bmatrix} \mathbf{0} \\ \boldsymbol{q} \\ \mathbf{0} \end{bmatrix}, \tag{7}$$

where $\boldsymbol{u}$ is the vector of the outward fluxes ordered cell-wise (with interior faces appearing twice with opposite sign), $\boldsymbol{p}$ are the cell pressures, and $\boldsymbol{\lambda}$ are the face pressures (without repetitions). The matrices $\boldsymbol{B}$ and $\boldsymbol{C}$ are block diagonal and the blocks corresponding to cell E are $\boldsymbol{T}_E^{-1}$ and $(1\,1\ldots1)^{\mathsf{T}}$ (length equal to the number of faces of E), respectively. Each column of $\boldsymbol{D}$ corresponds to a unique face and has one (for boundary faces) or two (for interior faces) unit entries corresponding to the index/indices of the face in the cell-wise ordering.

For the Stokes–Brinkman problem, Eq. 3, we will use the Taylor–Hood elements $\mathbb{P}_2/\mathbb{P}_1$ (i.e., linear elements in pressure space and quadratic elements in velocity space), which are a standard set of stable elements for the Stokes equations. The degrees-of-freedom for the two-dimensional Taylor–Hood elements are located at the vertices in the grid for pressure and for velocity they

are located at the vertices, at the midpoint of each cell edge, and at the cell centers. For completeness, we will take a closer look at the discrete system. Assuming the permeability tensor $\mathbf{K}$ is diagonal, we split the velocity $\vec{u}$ into its two spatial components u_1 and u_2. Letting $\{v_i\}$ and $\{\pi_i\}$ be the scalar Taylor-Hood basis functions, we can set $u_k = \sum_{\Omega_i} u_{ik} v_i$ and $p = \sum_{\Omega_i} p_i \pi_i$. The mixed system can then assembled in the form

$$\begin{bmatrix} \boldsymbol{B}_1 & \mathbf{0} & \boldsymbol{C}_1 \\ \mathbf{0} & \boldsymbol{B}_2 & \boldsymbol{C}_2 \\ \boldsymbol{C}_1^{\mathsf{T}} & \boldsymbol{C}_2^{\mathsf{T}} & \mathbf{0} \end{bmatrix} \begin{bmatrix} \boldsymbol{u}_1 \\ \boldsymbol{u}_2 \\ -\boldsymbol{p} \end{bmatrix} = \begin{bmatrix} \mathbf{0} \\ \mathbf{0} \\ \boldsymbol{q} \end{bmatrix}, \tag{8}$$

where $\boldsymbol{u}_1$ and $\boldsymbol{u}_2$ are vectors of the two velocity components u_{i1} and u_{i2}, respectively, and $\boldsymbol{p}$ is the vector of the pressure values p_i. Once again assuming no-flow boundary conditions, the entries in the matrices are

$$B_{ij,k} = \int_\Omega \mu\, v_i K^{-1}_{c,kk} v_j \, d\Omega + \int_\Omega \tilde{\mu} \left(\frac{\partial v_i}{\partial x_1} \frac{\partial v_j}{\partial x_1} + \frac{\partial v_i}{\partial x_2} \frac{\partial v_j}{\partial x_2} \right) d\Omega, \qquad C_{ij,k} = \int_\Omega \frac{\partial v_i}{\partial x_k} \pi_j \, d\Omega,$$

where $k = 1,\ 2$ denotes the spatial dimension and c denotes the respective cell.

The MsMFE Formulation. To define the MsMFE discretization for the Darcy equation, Eq. 1, we start by defining the coarse grid. Each block in this grid is defined as a connected collection of cells from the fine grid, that is, block number i is given as $\Omega_i = \bigcup_{k=1}^{N_i} E_k$ for some constant N_i. In the simplest case, the coarse grid is formed as a uniform partition of the fine Cartesian grid so that each block Ω_i becomes rectangular. Over this coarse grid, we define a discrete approximation space that generalizes RT0: the pressure is approximated by a constant in each block, whereas for the velocity we use a set of basis functions that are computed numerically and contain subcell resolution. Each basis function represents a unit flow over the interface between two coarse blocks, and hence there is one basis function associated with each pair of blocks in the coarse grid (Aarnes et al. 2006). Let Ω_{ij} be a neighborhood containing two neighboring blocks Ω_i and Ω_j. The basis function associated with the interface $\partial\Omega_i \cap \partial\Omega_j$ is constructed by solving the following flow problem over Ω_{ij}

$$\mu \mathbf{K}^{-1} \vec{\psi}_{ij} + \nabla \varphi_{ij} - \tilde{\mu} \Delta \vec{\psi}_{ij} = 0, \qquad \nabla \cdot \vec{\psi}_{ij} = \begin{cases} w_i(\vec{x}), & \text{if } \vec{x} \in \Omega_i, \\ -w_j(\vec{x}), & \text{if } \vec{x} \in \Omega_j, \\ 0, & \text{otherwise.} \end{cases} \tag{9}$$

Here $w_i(\vec{x})$ is a weight function that is normalized over Ω_i, whose purpose is to produce a flow with unit average flux over the interface $\partial\Omega_i \cap \partial\Omega_j$. To get a conservative method, we must choose w_i proportional to q in blocks containing nonzero source terms. In all other blocks, we may choose w_i more freely and the simplest choice is $w_i(\vec{x}) = 1/|\Omega_i|$. (We will return to w_i below.) To localize the basis functions, we impose no-flow boundary conditions $\vec{\psi}_{ij} \cdot \vec{n} = 0$ on $\partial\Omega_{ij}$. To motivate this construction of the basis functions $\vec{\psi}_{ij}$, let us first consider the case of pure Darcy flow in a 1-D homogeneous domain ($\tilde{\mu} = 0$ and $\mathbf{K} \equiv \mathbf{I}$). We define $w_i \equiv 1$, and set $\Omega_i = [-1, 0]$ and $\Omega_j = [0, 1]$. Then by solving Eq. 9, we obtain $\psi_{ij} = 1 - |x|$, which coincides with the RT0 velocity basis. When $\mathbf{K}$ has subscale variation, solving Eq. 9 gives generalized RT0 basis functions that account for the subscale variations in velocity, given a unit flux over the corresponding block interface.

The construction defined in Eq. 9 is general and can be performed for arbitrary connected collections of cells from the fine grid. If Ω_i and Ω_j are allowed to be polyhedral rather than rectangular, we compute the generalization of the RT0 basis functions to polyhedral blocks (Aarnes et al. 2006). The underlying fine grid can also be fully unstructured as discussed in more detail by Aarnes et al. (2008), who also suggest a set of simple guidelines for how to automatically define good coarse grids.

When the coarse blocks contain free-flow regions, the construction is entirely analogous, except that the basis functions are computed using Stokes–Brinkman equations rather than the Darcy equations used in the standard MsMFE method. Using normalized weight functions that scale with $\mathrm{trace}(\mathbf{K})$, we produce basis functions that correspond to a unit flow over the interface $\partial\Omega_i \cap \partial\Omega_j$ and account for the increased flow induced by the presence of free-flow regions within the coarse blocks. In the porous subdomains, this choice of w_i also means that we avoid unnaturally large velocities in low-permeable fine cells within the coarse blocks; see Aarnes et al. (2006) for more details. Notice, however, that setting $\tilde{\mu} = \mu$ in Eq. 9 and using Taylor–Hood elements to solve the local flow problem means that we introduce errors in the basis functions for the case of pure Darcy flow. In particular, for homogeneous permeability and rectangular support, we are no longer able to reproduce the RT0 basis functions exactly. **Fig. 1** displays basis functions for both a homogeneous and a vugular domain at an interface away from sources/sinks. The left figure shows that the basis function is almost identical to the corresponding RT0 velocity basis, also when solving Stokes–Brinkman equations using Taylor–Hood discretization.

Finally, we mention a few improvements that can be used to increase the accuracy of the multiscale approximation. If Ω_{ij} is chosen to be larger than $\Omega_i \cup \Omega_j$, we say that the basis function is computed using overlap or oversampling, which is introduced to lessen the impact of the no-flow boundary conditions that localize the basis functions. Similarly, it has been shown that it is advantageous to let the coarse blocks adapt to low-permeable objects like shales (Aarnes et al. 2006) or to long-range high-flow regions like fracture corridors (Natvig et al. 2009). Finally, if a better approximation is required for the pressure, one may also

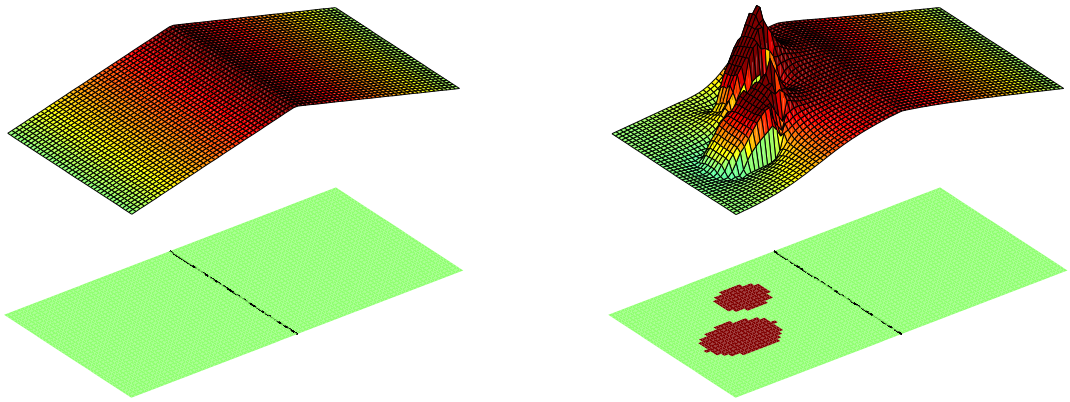

Fig. 1—The figure shows the x-component of two basis functions for an interface between two rectangular grid blocks plotted on top of the permeability. The left figure shows a completely homogeneous domain, and the right figure shows a homogeneous matrix with two high-permeable vugs. There are no sources or sinks in the plotted grid blocks.

utilize the pressures φ_{ij} from the local flow problems, Eq. 9, as additional basis functions; see Krogstad et al. (2009) for more details. Herein, however, our focus is on extending the MsMFE method to a multiphysics setting and we will therefore not use any of these more advanced constructions.

Coarse-Scale Hybrid System. Having constructed the multiscale basis functions, we are now in a position to assemble the global coarse-scale hybrid system. How to do this is thoroughly described by Krogstad et al. (2009) and Skaflestad and Krogstad (2008) for Darcy flow. Here, we will go briefly through the structure of the hybrid system and comment on a few issues that arise because of the fine-scale Stokes–Brinkman model and the use of Taylor–Hood elements.

Let $\boldsymbol{\psi}_{ij}$ denote the basis function resulting from solving Eq. 9. In previous formulations of the MsMFE method, the basis functions have been represented as a vector of fluxes defined on the set of cell-wise ordered *faces* in the fine grid representing Ω_{ij} (Krogstad et al. 2009). Using Taylor–Hood to compute basis functions, however, means that the basis functions are given in nodal points and must therefore be represented as a vector of cell-wise ordered *nodal* points in the fine grid. In this vector, a nodal point may belong to more than one Ω_{ij} and will then be represented more than once, each time with a different value. To define the multiscale hybrid system, we introduce a splitting of the basis functions, $\boldsymbol{\psi}_{ij} = \boldsymbol{\psi}^H_{ij} - \boldsymbol{\psi}^H_{ji}$ such that $\boldsymbol{\psi}^H_{ij}(E)$ equals $\boldsymbol{\psi}_{ij}(E)$ if $E \in \Omega_{ij} \setminus \Omega_j$ and is zero otherwise, and $\boldsymbol{\psi}^H_{ji}(E)$ equals $-\boldsymbol{\psi}_{ij}(E)$ if $E \in \Omega_j$ and is zero otherwise. Next, we arrange all the *hybrid* basis functions $\boldsymbol{\psi}^H_{ij}$ as columns in a matrix $\boldsymbol{\Psi}$. To account for the fact that the basis functions are velocities and not fluxes, we have to multiply with the inverse of the area matrix $\boldsymbol{A}^{-1}$. Then the hybrid multiscale system reads,

$$\begin{bmatrix} (\boldsymbol{A^{-1}})^{\mathsf{T}}\boldsymbol{\Psi}^{\mathsf{T}}\boldsymbol{B}^f_D\boldsymbol{\Psi}\boldsymbol{A^{-1}} & \boldsymbol{C} & \boldsymbol{D} \\ \boldsymbol{C}^{\mathsf{T}} & \boldsymbol{0} & \boldsymbol{0} \\ \boldsymbol{D}^{\mathsf{T}} & \boldsymbol{0} & \boldsymbol{0} \end{bmatrix} \begin{bmatrix} \boldsymbol{u}^c \\ -\boldsymbol{p}^c \\ \boldsymbol{\lambda}^c \end{bmatrix} = \begin{bmatrix} \boldsymbol{0} \\ \boldsymbol{q}^c \\ \boldsymbol{0} \end{bmatrix}. \tag{10}$$

Here, $\boldsymbol{C}$ and $\boldsymbol{D}$ are constructed from the coarse-grid as for Eq. 7, and the vectors $\boldsymbol{u}^c$, $\boldsymbol{p}^c$, and $\boldsymbol{\lambda}^c$ contain the coarse-scale degrees-of-freedom. The matrix $\boldsymbol{B}^f_D$ is the fine-scale analogue of Eq. 7 defined with Taylor–Hood elements rather than RT0, and is a block diagonal matrix of 9×9 blocks for 2D Cartesian grids. If we use no overlap, the B-part of Eq. 10 is block diagonal with respect to the coarse blocks and can be reduced to a symmetric positive-definite system for $\boldsymbol{\lambda}^c$. When overlap is used, one is in general better off using a mixed formulation of the system.

Once the solution of Eq. 10 is computed, the fine-scale velocities can be computed as $\boldsymbol{u}^f = \boldsymbol{\Psi}\boldsymbol{u}^c$, where one must remember that each nodal point may have contributions from more than one basis function on the coarse grid.

Numerical Experiments

Darcy Flow. Our first test of the multiscale Darcy/Stokes–Brinkman method is on a sandstone reservoir for which the Darcy flow model is applicable. To this end, we will use Model 2 from the Tenth SPE Comparative Solution Project (Christie and Blunt 2001). The purpose of this test is threefold:

- we want to determine how well the Darcy equations are solved using Taylor–Hood elements compared with the usual Raviart–Thomas elements;
- we want to calculate the influence of the Stokes part of the Stokes–Brinkman equation on regular Darcy flow;

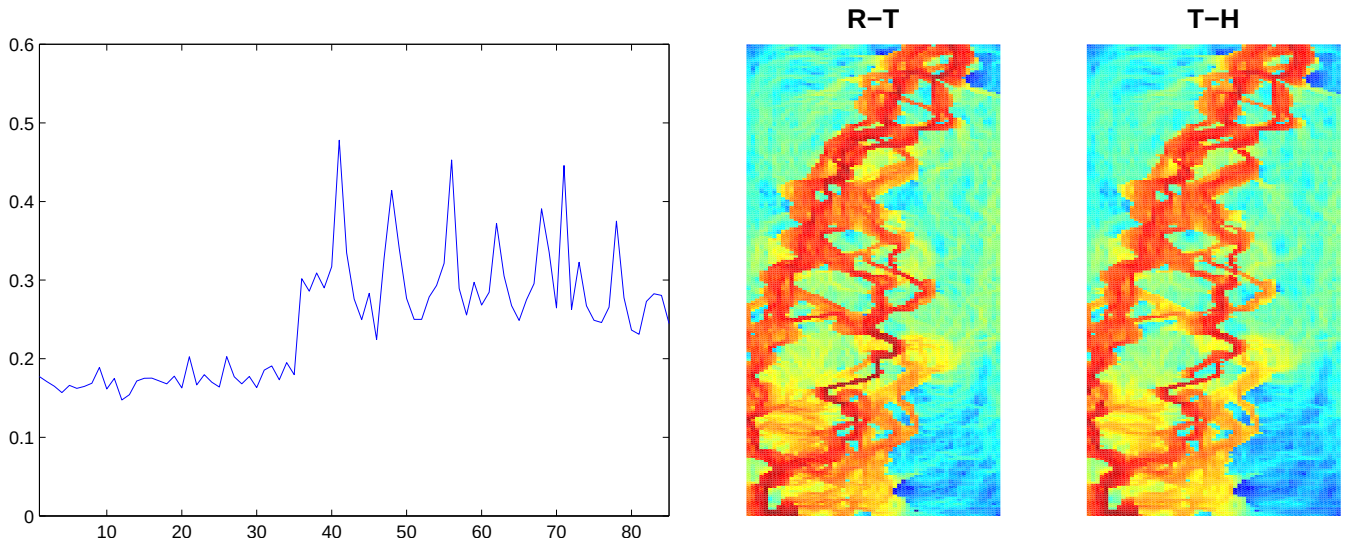

Fig. 2—The left figure shows the discrepancy in the flux computed by the Raviart–Thomas and the Taylor–Hood discretizations measured in a relative L^2 norm for the 85 layers of the SPE 10 model. The middle and right figures display logarithmic Darcy flow velocities from the layer with the highest flux discrepancy (Layer 41) computed with Raviart–Thomas and Taylor–Hood elements, respectively.

- we want to asses the accuracy of Darcy/Stokes–Brinkman multiscale simulations versus Stokes–Brinkman fine-scale simulations in the porous (matrix) part of a vuglar medium.

We start off by comparing the Raviart–Thomas and the Taylor–Hood discretization on each of the 85 layers of the SPE 10 model. Setting $\tilde{\mu} = 0$ excludes the Stokes part ($\tilde{\mu}\Delta\vec{u}$) of the equation, so that we are left with only the original Darcy equation, Eq. 1. In each layer, we place one injector in the cell with the highest permeability along the lower edge of the reservoir and a producer in the cell with the highest permeability along the upper edge. For the Raviart–Thomas discretization, each well is modeled as a source/sink term distributed over the whole cell. In the Taylor–Hood discretization, the sources/sinks are set in the pressure nodes. In both cases we impose no-flow conditions on all sides.

To compare the two discretizations, we assume that one is only interested in the fluxes over each cell face and will therefore compare the accuracy in edge fluxes rather than the pointwise accuracy of the velocities. For the Raviart–Thomas discretization, the fluxes correspond directly to the degrees-of-freedom and will be denoted by $\boldsymbol{u}_k^{RT}$ for cell k. For the Taylor–Hood discretization, we have to integrate the velocity approximation over the cell faces to derive fluxes $\boldsymbol{u}_k^{TH}$ (i.e., average the three degrees-of-freedom associated with the normal velocity component at each face). We then measure the discrepancy e_u in terms of a relative L^2 norm as follows:

$$e_u = \sqrt{\frac{\sum_{k=1}^{N} \|\boldsymbol{u}_k^{RT} - \boldsymbol{u}_k^{TH}\|}{\sum_{k=1}^{N} \|\boldsymbol{u}_k^{RT}\|}}. \tag{11}$$

The left plot in **Fig. 2** shows this error for all 85 layers of the SPE 10 model. For the smooth upper layers in the Tarbert formation, the error oscillates around 0.20, and for the fluvial bottom layers it increases to a mean of 0.32. The middle and right subfigures show logarithmic plots of the velocity in the layer with the highest flux discrepancy (Layer 41). Some of the discrepancy, in particular in the near-well zones, can be attributed to the different placement of sources/sinks in the two discretizations. However, the results also demonstrate the level of error inherent in the fine-scale solution, which people often mistakenly tend to consider as the *correct* solution.

To determine the influence of the Stokes term in the Stokes–Brinkman equation for a typical Darcy flow, we compared simulations of the 85 layers using the Taylor–Hood elements with $\tilde{\mu} = 0$ and with $\tilde{\mu} = \mu$. The results show a relative error of the velocity (and not the flux) measured in all nodal points in the order of 10^{-11}, so for normal permeability values (here in the order of 10^{-4} mD to 10 D) and typical reservoir dimensions (here $1200 \times 2200 \times 170$ ft), the Stokes term is negligible.

In the last test of this example, we will compare solutions computed with our multiscale Darcy/Stokes–Brinkman method with fine-scale Stokes–Brinkman solutions. For each layer, we compare three different coarse grids with 3×11, 6×22, and 12×44 blocks. **Fig. 3** reports the relative errors of the velocity for all 85 layers. We see that for the top 35 layers, the velocity error is quite small and at the same level as the error in Fig. 2. For the different coarsening degrees (starting with the 3×11) the mean norms are 0.20, 0.18 and 0.22. For the 50 bottom layers, the flux norm reaches about twice as high values: 0.37, 0.52 and 0.44. With a few exceptions, it seems that the coarser grids generally give better results than the finer grids for the multiscale method. For this particular case, the flow patterns are highly influenced by long-range correlations. For coarse grids with few but large

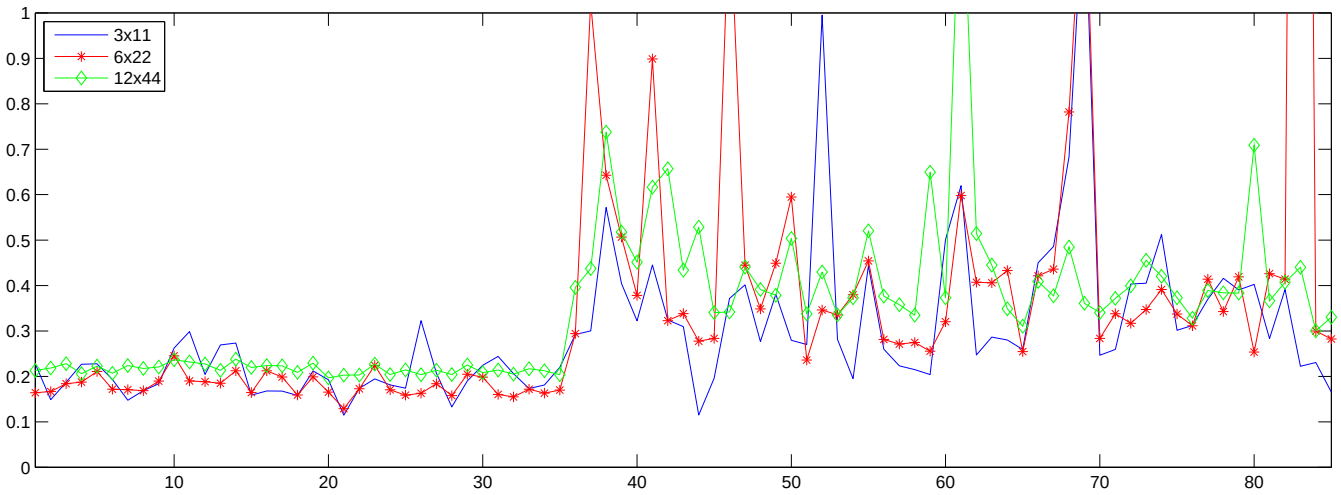

Fig. 3—Multiscale simulations for the 85 layers of the SPE 10 model. The figure shows the relative L^2 discrepancy of the fine-scale velocities for a fine-scale simulation versus multiscale simulations for three different coarse grids. The discrepancy for the 3×11 coarse grid is plotted in blue, the 6×22 grid in red, and the 12×44 grid in green.

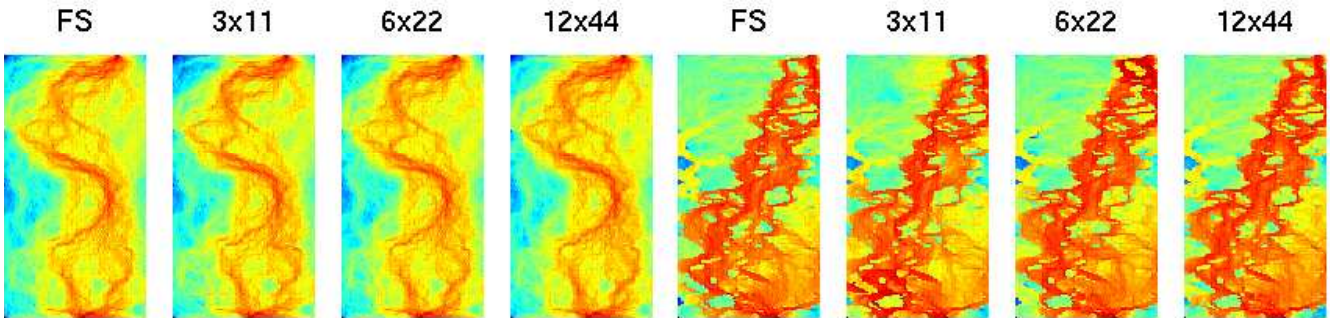

Fig. 4—Multiscale simulations of Layer 21 (left) and Layer 69 (right) of the SPE 10 model. The figure compares fine-scale velocities computed directly on the fine scale (FS) with multiscale simulations for three different coarse grids.

blocks, these long-range correlations are resolved in the basis functions, whereas for coarse grids with many small blocks, the long-range correlations must be resolved by the global system. **Fig. 4** compares the fluxes in the layers with least (Layer 21) and largest (Layer 69) errors. For Layer 21, it is difficult to distinguish the three multiscale simulations from the fine-scale reference solution. For Layer 69, we see that the flow channels are very well reproduced in the multiscale simulations, but the amount of flow in each channel varies slightly. These results are in accordance with the comparisons of multiscale methods for Darcy flow as reported by Kippe et al. (2008).

Vuggy and Fractured Reservoirs. The purpose of introducing the Stokes–Brinkman equation in the multiscale method was to perform detailed modeling of vuggy and naturally-fractured reservoirs. In this subsection we show examples of how well the fine-scale Stokes–Brinkman flow in vuggy and fracture networks is represented within a coarse-scale Darcy flow model using multiscale elements.

We consider three different models of vugular and fractured media. All models have 200×200 grid cells with each grid cell modeling 10×10 cm. In the multiscale discretization, each domain is divided into 5×5 coarse grid blocks. The fluid under consideration is water, with $\mu = 1cP$. The sources and sinks are set in every node on the left and right side, respectively, except in the vertices of the coarse grid blocks.

In the first model we have randomly distributed 26 vugs with sizes of 1.8–10.4 m^2 (diameters of 70 – 220 cm) in the homogeneous matrix (see **Fig. 5**). The matrix permeability has a value of 1 Darcy, while the permeability in the vugs is set to be 10^7 times higher. In the second model, we consider a domain with fourteen long-range fractures that are straight lines in the vertical and horizontal directions, with apertures of 10 cm and lengths of 300–900 cm (see **Fig. 6**). The third model combines the first two models, getting a vugular medium in which some of the vugs are connected by long-range fractures (see **Fig. 7**). In all three permeability plots we clearly see the high-permeable vugs and fractures in red, and the coarse-grid partitioning is shown in yellow.

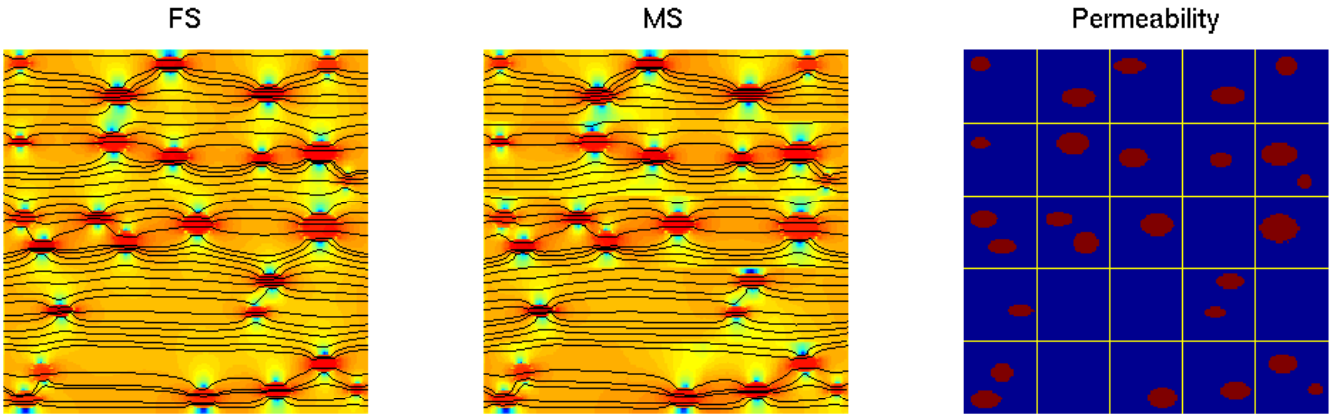

Fig. 5—Simulations of a vuggy reservoir with a homogeneous matrix. The left and middle plots show the logarithmic velocity for the fine-scale (FS) and the multiscale (MS) solutions, respectively, overlaid by streamlines. The right plot shows the permeability with high-permeable vugs in red and the coarse-grid partitioning in yellow.

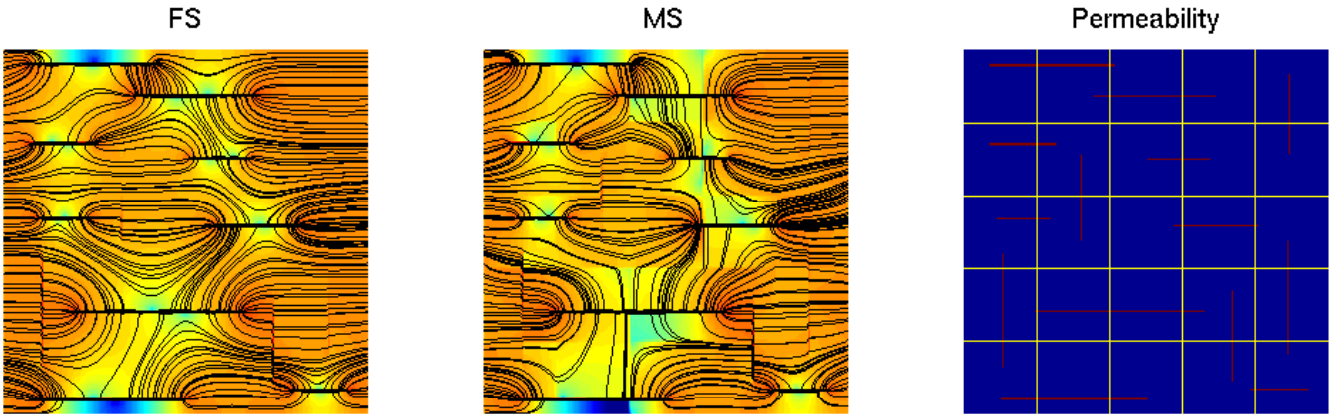

Fig. 6—Simulations of a reservoir with a homogeneous matrix and high permeable fractures. The left and middle plots show the logarithmic velocity for the fine-scale (FS) and the multiscale (MS) solutions, respectively, overlaid by streamlines. The right plot shows the permeability with high-permeable fractures in red and the coarse-grid partitioning in yellow.

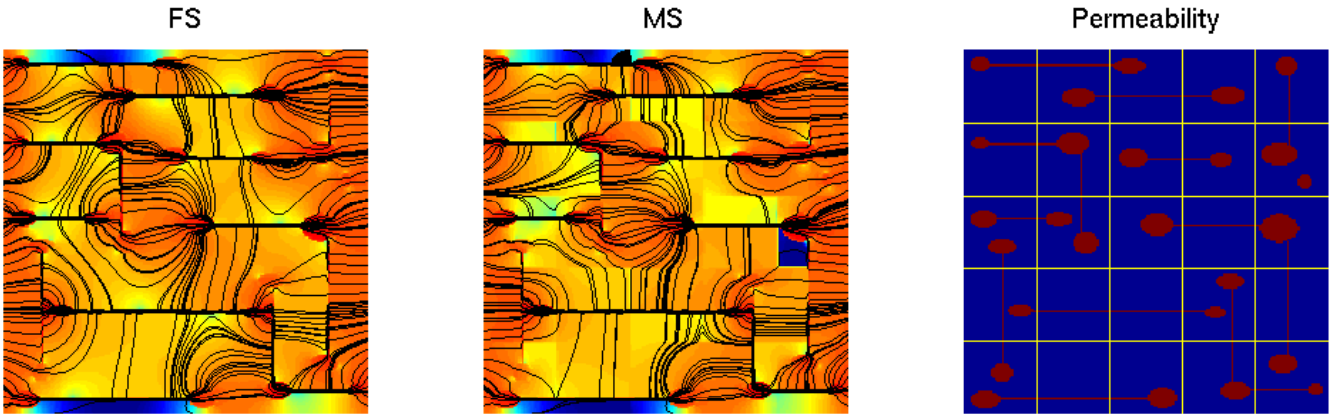

Fig. 7—Simulations of a vuggy reservoir with a homogeneous matrix and high-permeable fractures. The left and middle plots show the logarithmic velocity for the fine-scale (FS) and the multiscale (MS) solutions, respectively, overlaid by streamlines. The right plot shows the permeability with high-permeable vugs and fractures in red and the coarse-grid partitioning in yellow.

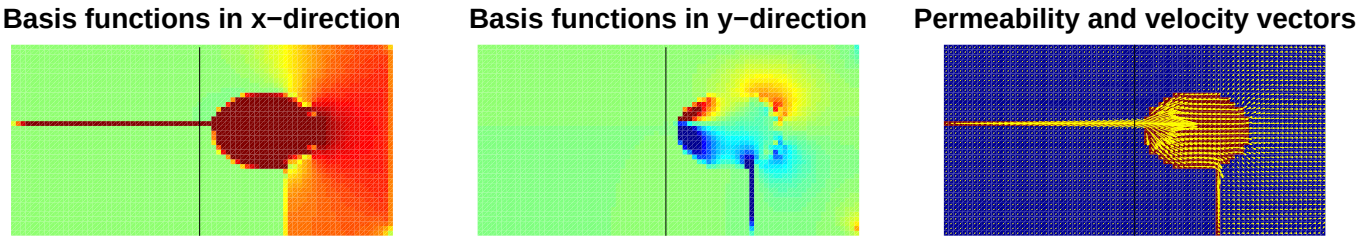

Fig. 8—Basis function associated with the interface between coarse blocks (4,3) and (5,3).

In Fig. 5, we have plotted the fine-scale velocities obtained by solving the Stokes–Brinkman directly on the fine-scale model along with the fine-scale velocities computed by our Darcy/Stokes–Brinkman multiscale method. On top of the velocity plots we have drawn streamlines to better visualize the flow. The model can be characterized as having short correlation lengths in the sense that the each free-flow vug is confined to a single coarse block. Numerous simulations of similar type have shown that the multiscale method is able to reproduce flow of this type with good accuracy. For the model in Fig. 5, the velocity error is only 0.06 in the relative L^2 norm.

The second model has somewhat longer correlation lengths in the form of vertical and horizontal fractures that typically penetrate a few consecutive blocks. (The longest fracture penetrates blocks (1,2) to (4,2), where block (1,1) is in the lower left corner.) The multiscale method is still able to deliver reasonable accuracy, with velocity errors about 0.1 in the relative L^2 norm, although the streamline plots reveal some qualitative differences. In the third model, some of the vugs are connected by fractures and this gives longer correlations in the form of free-flow regions that extend in both coordinate directions; an example is the continuous free-flow region that extends from block (3,3) to block (5,1). The velocity error is about 0.1 also for this model, but the qualitative differences are now easier to spot.

In an effort to explain the somewhat larger errors observed when free-flow regions extend beyond a single block, we focus on coarse block number (5,3), which is the rightmost block in the middle row of Fig. 7. This block has the largest discrepancy between the fine-scale and the multiscale solutions. When using the multiscale method, the velocities within each coarse block are determined by the basis functions. We therefore look at the basis functions obtained when solving the local system defined by blocks (4,3) and (5,3). **Fig. 8** displays the basis functions in both the x- and the y-direction. Since the weight function w_i scales with $\mathrm{trace}(\mathbf{K})$, the cells in the fracture will be assigned a weight that is 10^7 time higher than in the surrounding cells, meaning that the sources in the non-fractured cells in the left half of the local domain are effectively set to zero. Since the right-hand block is at the boundary of the domain where the sinks are placed, the weight function is nonzero only for cells at the right edge. Altogether, this setup leads to the flow seen in the quiver plot in the right plot in Fig. 8. In block (4,3), the flow is driven through the fracture, and when it enters block (5,3), it continues into the vug and then spreads out towards the sink cells at the right edge. Some of the flow continues down the vertical fracture and is driven towards the right edge from there. In effect, this means that the background flow in the matrix is not represented by this basis function in large parts of the local domain, which leads to the blue no-flow region seen in block (5,3) of the multiscale solution in Fig. 7. A similar behavior has been seen in a wide variety of models run by the authors.

For fractures extending beyond a single block in the *diagonal* direction, numerous experiments demonstrate the opposite effect, namely that the multiscale method introduces large flow in the porous region surrounding the fracture. This can be explained as follows: suppose a fracture connects blocks (i, j) and $(i + 1, j + 1)$. Since the MsMFE method only represents coarse-scale flow between coarse blocks sharing a common face, the flow from block (i, j) to block $(i + 1, j + 1)$ must make a detour in blocks $(i + 1, j)$ and/or $(i, j + 1)$. The same effect has been observed previously for pure Darcy flow and is discussed in more detail by Kippe et al. (2008).

To overcome the problem of fractures extending beyond a single block, one can introduce extra coarse blocks that represent the long-range fractures. In Fig. 8 this amounts to splitting block (4,3) into three blocks that all are coupled with block (5,3) and together take care of the flow in the fracture and in the porous region above and below the horizontal fracture. The efficiency of this approach has been demonstrated by Natvig et al. (2009), but has so far not been implemented in our simple Darcy/Stokes–Brinkman multiscale solver.

Concluding Remarks

In this paper we have developed a multiphysics version of the mixed finite-element method in which the Stokes–Brinkman equations are used to compute basis functions to be used in a Darcy flow model on a coarse scale. The new methodology was applied to two examples. First, we considered a *strongly* heterogeneous sandstone reservoir (Model 2 from the SPE 10 benchmark), for which we demonstrated that the effect of the second-order term in the Stokes–Brinkman models is negligible and that the errors introduced when using the multiscale method are of the same order-of-magnitude as the discrepancy observed between the Raviart–Thomas and Taylor–Hood discretizations of the fine-scale Darcy equations.

In the second example, we considered three simplified 2-D models of fractured and vugular media that are typical for a large

number of experiments run by the authors. When free-flow regions are confined to a single coarse block, the multiscale method delivers qualitatively correct solutions with good accuracy. If the free-flow regions extend beyond a single coarse block, the multiscale method is able to reproduce major parts of the flow patterns, but to get all small details correct, one may have to introduce an adaptive coarsening in which free-flow regions are represented as extra coarse blocks (as discussed by Aarnes et al. (2006) for long-correlation shale objects and by Natvig et al. (2009) for fracture corridors). This is a topic of ongoing research.

Although the Stokes–Brinkman model is a promising approach for simulating vugular and naturally-fractured reservoirs, its discretization using the Taylor–Hood elements is relatively costly because of the high number of degrees of freedom. Hence, flow problems may fast become computationally intractable with increasing model sizes, in particular in 3-D. The multiscale method developed herein has a natural parallelism in the computation of basis function and also has a potential for reduced memory requirements, and may therefore be an efficient approach for attacking high-resolution 3-D models.

Acknowledgments

The authors gratefully acknowledge financial support from Shell Norge AS and the Research Council of Norway under grant number 175962/S30. We also thank Peter Popov and Dr. Yalchin Efendiev for helpful discussions.

Nomenclature

Physical quantities:

f	=	body force term
$\mathbf{K}$	=	absolute permeability
p	=	pressure
$\vec{u}$	=	velocity
$\vec{x}$	=	spatial coordinate
q	=	volumetric rate
μ	=	viscosity
$\tilde{\mu}$	=	effective viscosity

Domain and grid:

Ω	=	entire physical domain
∂D	=	boundary of domain D
E	=	cell in the fine grid
Ω_i	=	coarse block number i
Ω_{ij}	=	support for basis function $\vec{\psi}_{ij}$

Basis functions, etc:

$\vec{v}$	=	test function for velocity on fine scale
π	=	test function for pressure on fine scale
$\vec{\psi}_{ij}$	=	basis function on interface of block i and j
$\vec{\psi}_{ij}^{H}$	=	hybrid split of basis function
ϕ_{ij}	=	pressure associated with $\vec{\psi}_{ij}$
w_i	=	weight function associated with coarse block Ω_i

Vectors and matrices:

$\boldsymbol{p}$	=	vector of cell/block pressures
$\boldsymbol{\lambda}$	=	vector of face pressures
$\boldsymbol{u}$	=	vector of outward fluxes on cell/block faces
$\boldsymbol{B}$	=	inner product of velocity basis functions
$\boldsymbol{C}$	=	integral of divergence of velocity b.f.
$\boldsymbol{D}$	=	mapping from local to global faces numbering
$\boldsymbol{T}_E$	=	transmissibility matrix for cell E
$\boldsymbol{\Psi}$	=	matrix of all basis functions

Numbers:

N	=	number of cells in fine grid
N_i	=	number of cells in coarse block Ω_i

Subscripts:

i, j, k	=	block/cell numbers
D, S	=	Darcy and Stokes
SB	=	Stokes–Brinkman
c, f	=	coarse/fine grid

References

Aarnes, J. E. 2004. On the Use of a Mixed Multiscale Finite Element Method for Greater Flexibility and Increased Speed or Improved Accuracy in Reservoir Simulation. *Multiscale Model. Simul.*, 2(3):421–439 (electronic).

Aarnes, J. E., Krogstad, S., and Lie, K.-A. 2006. A Hierarchical Multiscale Method for Two-Phase Flow Based Upon Mixed Finite Elements and Nonuniform Coarse Grids. *Multiscale Model. Simul.*, 5(2):337–363 (electronic).

Aarnes, J. E., Krogstad, S., and Lie, K.-A. 2008. Multiscale Mixed/Mimetic Methods on Corner-Point Grids. *Comput. Geosci.*, 12(3):297–315. Doi:10.1007/s10596-007-9072-8.

Arbogast, T. and Brunson, D. S. 2007. A Computational Method for Approximating a Darcy–Stokes System Governing a Vuggy Porous Medium. *Comput. Geosci.*, 11(3):207–218.

Arbogast, T. and Gomez, M. S. M. 2008. A Discretization And Multigrid Solver for a Darcy–Stokes System of Three Dimensional Vuggy Porous Media. *submitted*.

Arbogast, T. and Lehr, H. L. 2006. Homogenization of a Darcy–Stokes System Modeling Vuggy Porous Media. *Comput. Geosci.*, 10(3):291–302.

Chen, Z. and Hou, T. 2003. A Mixed Multiscale Finite Element Method for Elliptic Problems With Oscillating Coefficients. *Math. Comp.*, 72:541–576.

Christie, M. A. and Blunt, M. J. 2001. Tenth SPE Comparative Solution Project: A Comparison of Upscaling Techniques. *SPE Reservoir Eval. Eng.*, 4:308–317. Url: `http://www.spe.org/csp/`.

Hajibeygi, H., Bonfigli, G., Hesse, M. A., and Jenny, P. 2008. Iterative Multiscale Finite-Volume Method. *J. Comput. Phys*, 227(19):8604–8621.

Hou, T. and Wu, X.-H. 1997. A Multiscale Finite Element Method for Elliptic Problems in Composite Materials and Porous Media. *J. Comput. Phys.*, 134:169–189.

Juanes, R. and Tchelepi, H. A. 2008. Special Issue on Multiscale Methods for Flow and Transport In Heterogeneous Porous Media. *Comput. Geosci.*, 12(3):255–416.

Karper, T., Mardal, K.-A., and Winther, R. 2008. Unified Finite Element Discretizations Of Coupled Darcy–Stokes Flow. *Numer. Meth. PDEs*. Doi: 10.1002/num.20349.

Kippe, V., Aarnes, J., and Lie, K.-A. 2008. A Comparison Of Multiscale Methods for Elliptic Problems in Porous Media Flow. *Comput. Geosci.*, 12(3):377–398. Doi: 10.1007/s10596-007-9074-6.

Krogstad, S., Lie, K.-A., Nilsen, H. M., Natvig, J. R., Skaflestad, B., and Aarnes, J. E. 2009. A Multiscale Mixed Finite-Element Solver for Three-Phase Black-Oil Flow. Paper SPE 118993, presented at SPE Reservoir Simulation Symposium, The Woodlands, TX, USA, 2–4 February.

Lee, S. H., Wolfsteiner, C., and Tchelepi, H. 2008. Multiscale Finite-Volume Formulation for Multiphase Flow in Porous Media: Black Oil Formulation Of Compressible, Three Phase Flow With Gravity. *Comput. Geosci.*, 12(3):351–366. Doi:10.1007/s10596-007-9069-3.

Natvig, J. R., Skaflestad, B., Bratvedt, F., Bratvedt, K., Lie, K.-A., Laptev, V., and Khataniar, S. K. 2009. Multiscale Mimetic Solvers for Efficient Streamline Simulation of Fractured Reservoirs. Paper SPE 119132, presented at 2009 SPE Reservoir Simulation Symposium, The Woodlands, Texas, USA, 2–4 February.

Popov, P., Bi, L., Efendiev, Y., Ewing, R. E., Qin, G., Li, J., and Ren, Y. 2007. Multi-physics and Multi-scale Methods for Modeling Fluid Flow Through Naturally-Fractured Vuggy Carbonate Reservoirs. Paper SPE 105378, presented at 15^{th} SPE Middle East Oil & Gas Show and Conference, Bahrain, 11–14 March.

Popov, P., Efendiev, Y., and Qin, G. 2008. Multiscale Modeling and Simulations of Flows in Naturally Fractured Karst Reservoirs. *Commun. Comput. Phys.* In press.

Skaflestad, B. and Krogstad, S. 2008. Multiscale/Mimetic Pressure Solvers With Near-Well Grid Adaption. In *Proceedings of ECMOR XI–11th European Conference on the Mathematics of Oil Recovery*, number A36, Bergen, Norway. EAGE.

Wu, Y.-S., Qin, G., Ewing, R. E., Efendiev, Y., Kang, Z., and Ren, Y. 2006. A Multiple-Continuum Approach for Modeling Multiphase Flow in Naturally Fractured Vuggy Petroleum Reservoirs. Paper SPE 104173, presented at SPE International Oil & Gas Conference and Exhibition, Beijing, China, 5–7 December.

Zhou, H. and Tchelepi, H. 2008. Operator-Based Multiscale Method for Compressible Flow. *SPE J.*, 13(2):267–273.